Exploring the Earth

NORSAR Scientific Report No.2-2014

Semiannual Technical Summary

1 July – 31 December 2014

Tormod Kværna (Ed.)

Kjeller, August 2015

NORSAR

6.3 Stratospheric and Thermospheric Infrasound Signals Recorded at IS37

6.3.1 Introduction

The IMS infrasound array IS37 near Bardufoss in northern Norway, started providing data in October 2013. In August and September 2014, IS37 recorded for the first time infrasound signals from each of 15 ammunition destruction explosions at Hukkakero, a military site in Northern Finland at a distance of approximately 320 km.

The first 12 of the explosions were large blasts with yields of approximately 20 tons and, for each of these events, an extensive wavetrain is recorded. Approximately 18 minutes after the explosion, a long duration signal rich in high frequencies, is observed. Between 3 and 4 minutes later, signals of far shorter duration and lower frequency are observed with higher trace velocities, indicating refraction from greater altitudes.

Modelling supports the hypothesis that these distinct parts of the wavetrain are stratospheric and mesospheric/thermospheric phases respectively. We observe that the trace velocity for almost all of the stratospheric part of the wavetrain is essentially constant, whereas the thermospheric phases are associated with quite differing trace velocities: indicative of turning points at different altitudes.

The final three explosions at Hukkakero in 2014 were of far lower yield and only generated signal detections at IS37 in the stratospheric part of the wavetrain.

In this study we attempt to interpret features of the observed wavetrains, like the trace velocities and celerities, through modelling in perturbed atmospheric models. One goal for this study is to be able to create so-called celerity expectation lookup tables applicable for use in event location algorithms.

6.3.2 Hukkakero ground truth explosions in 2014

Between August 22 and September 3 in 2014, the Finnish military set off 15 explosions to demolish ammunition at the Hukkakero site in Northern Finland. All explosions occur within approximately 150 meters of the coordinates 67.934^{o}N 25.832^{o}E. The location of the explosion site in relation to the ARCI and IS37 infrasound arrays is displayed in Figure 6.3.1. Acoustic signals generated by Hukkakero blasts in previous years, recorded at other stations, have been considered by e.g. Gibbons et al. (2007, 2015), Israelsson (2013), and Liszka and Kværna (2008). Figure 6.3.2 shows observations at the IS37 central sensor of the 15 Hukkakero explosions in 2014. The leftmost part of each trace has been overlaid with the seismic recording at ARCES, colored red, which was used for detection and timing of the events and for associating the signals unambiguously with the source location. The apparent velocities of the infrasound signals arriving at IS37 are represented by the color background. It is clear that there are two distinct parts of the infrasonic wavetrain for these events. A long duration signal from around 18 to 20 minutes after the explosion time is rich in high frequency energy and arrives with an almost constant apparent velocity of the order of 340 m/s. Between 20 and 23 minutes after the explosion times, shorter duration signals are observed with lower frequency content. These arrive with higher apparent velocities and there is a significantly greater variability in the trace velocity, indicating ray turning points at different altitudes. The signal characteristics of the earlier and later parts of the wavetrain are consistent with those associated with stratospheric and

thermospheric returns respectively (Mutschlecner and Whitaker, 1999; Whitaker and Mutschlecner, 2008).

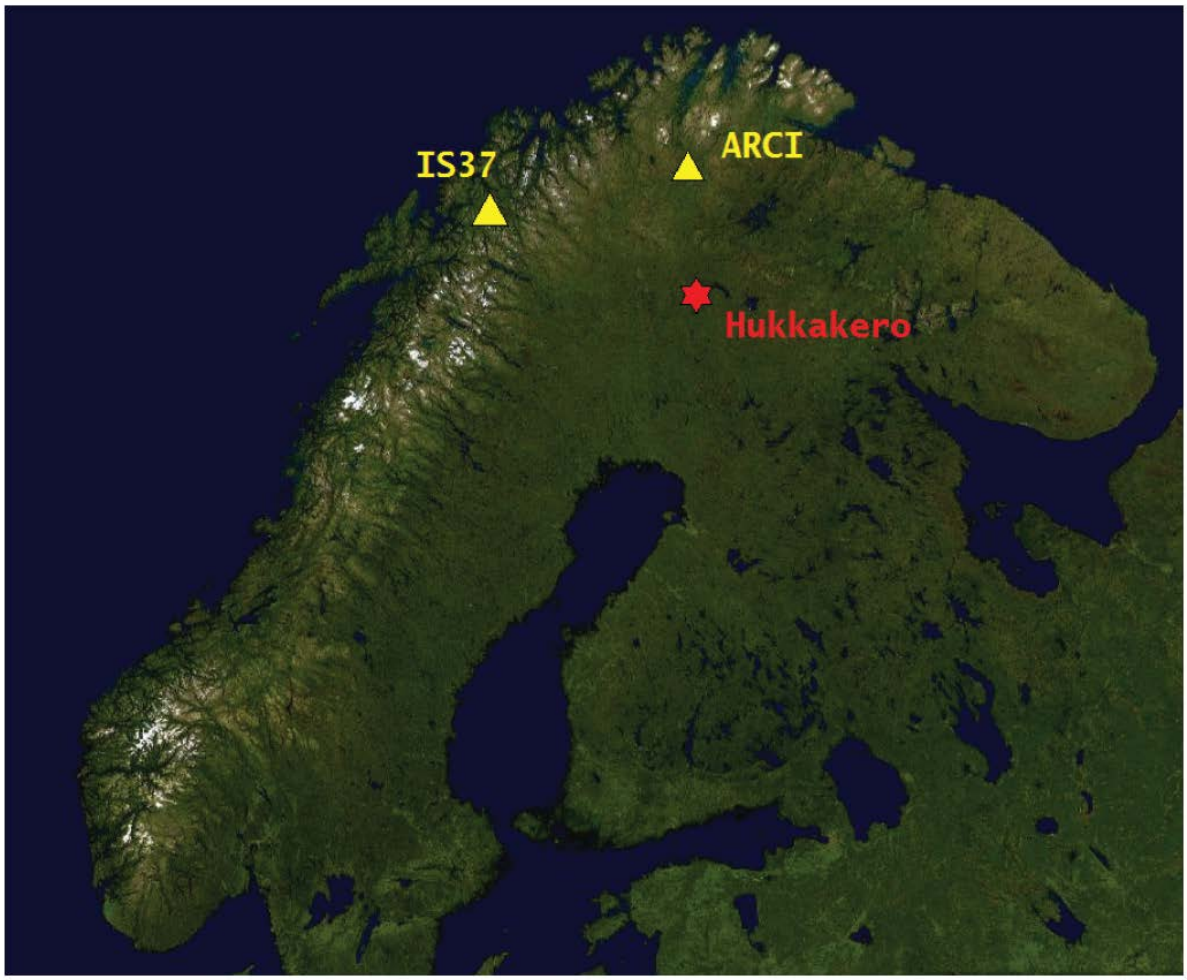

Fig. 6.3.1 Map showing the location of the explosion site at Hukkakero (67.934°N, 25.832°E) in relation to the infrasound arrays ARCI (69.538°N, 25.5078°E) and IS37 (69.0741°N, 18.6076°E).

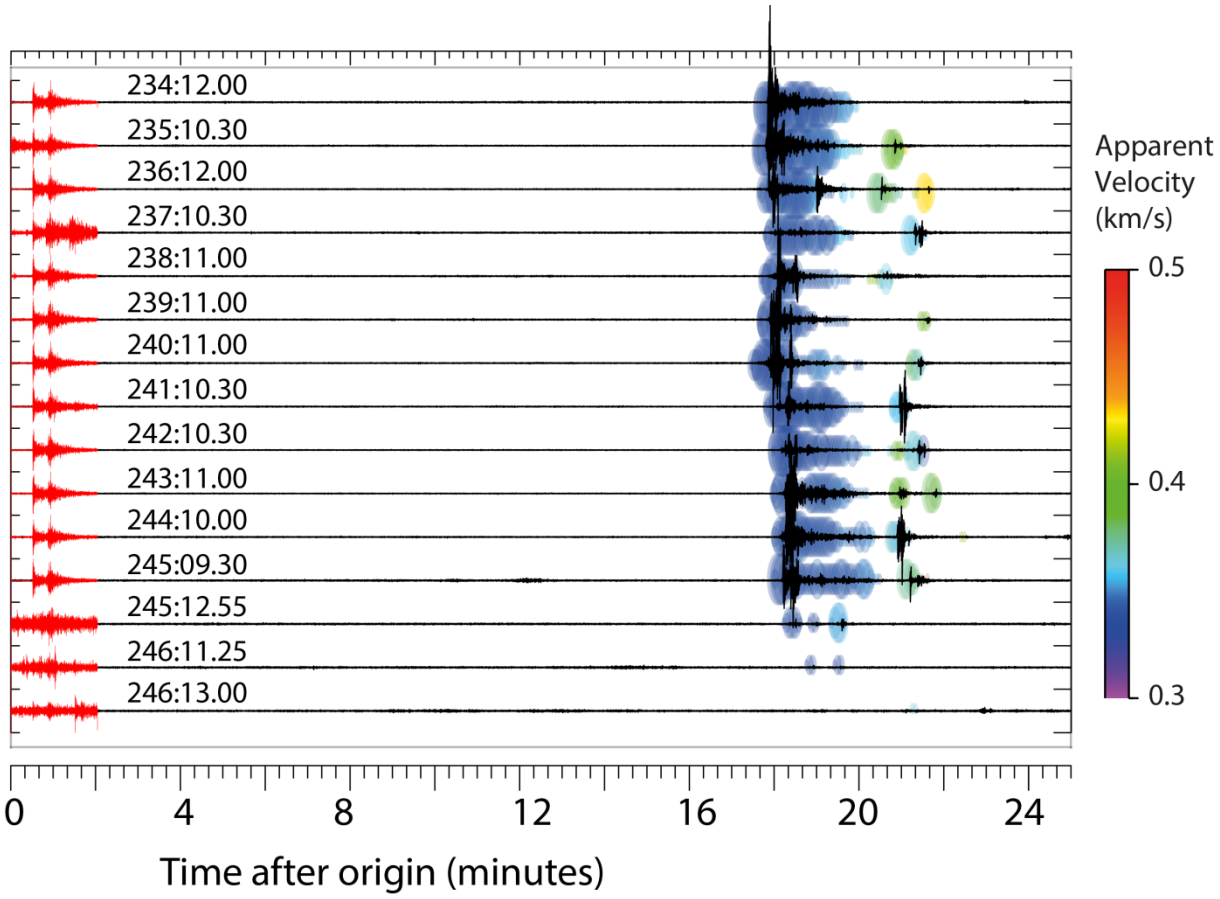

Fig. 6.3.2 Microbarograph data (1-4 Hz) at the IS37 central site (black) and seismic data (4-16 Hz) at the ARCES central site (red) for 15 Hukkakero events in 2014. The symbols behind the waveforms indicate the apparent velocity measured at IS37 and are sized proportional to the cross-correlation stack peak, provided consistency with a relevant infrasound signal. The cross-correlation values range between over 0.9 for the strongest signals to around 0.1 for signals right at the noise level. The first 12 events have a presumed explosive yield of approximately 20T, the final 3 are far smaller. The origin time is given to the nearest minute in the format ddd:hh.mm where ddd, hh, and mm are the day of year, the hour, and minute respectively. All waveforms are aligned using the seismic signals.

Figure 6.3.3 provides a closer look at the infrasonic signals recorded in the time-window 17 to 23 minutes following the blasts. The traces are filtered in a much broader frequency band (0.03 – 1.50 Hz) and show more clearly the differing frequency content of the two parts of the wavetrain. Instead of the trace from a single sensor, as is displayed in Figure 6.3.2, we show a beam of all 10 traces from the array steered with a backazimuth of 110 degrees and with an apparent velocity of 0.4 km/s. The beamforming provides a significant improvement in the signal-to-noise ratio (SNR) even though the constant apparent velocity chosen will not provide optimal waveform alignment for all parts of the wavetrain. The N- and U-shapes observed in the second part of the wavetrain typically result from nonlinear propagation and caustic effects (see, for example, Gainville et al., 2009).

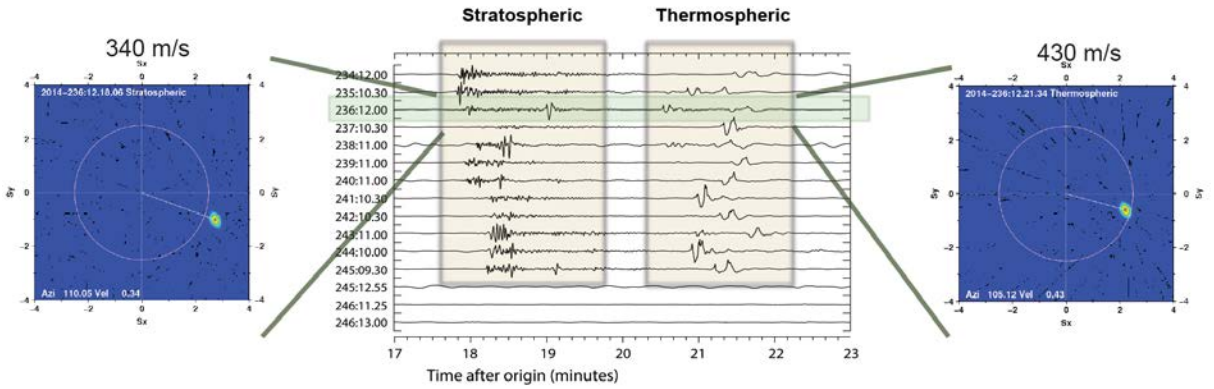

Fig. 6.3.3 Close in view of the infrasonic wavetrain at IS37 with a beam displayed for each of the events displayed in Figure 6.3.2. The beam is steered with an apparent velocity of 400 m/s and a backazimuth of 110 degrees and the waveforms displayed are filtered in the frequency band 0.03 Hz to 1.5 Hz. The slowness estimates are calculated using the channel to channel correlation procedure of Brown et al. (2002) in the 1-4 Hz frequency band.

6.3.3 Construction of atmospheric models for ray-tracing

We wish to use ray-tracing to model the infrasound propagation from the explosion site to the IS37 array. For this, we need both a ray-tracing algorithm and atmospheric specifications at the times of the events. The ray-tracing software used is ART2D (Walker, 2012), as used in Hedlin and Walker (2013). Using a philosophy akin to the one underlying the Ground-to-Space (G2S) model (Drob et al. 2003, 2010), we construct a compound model of the atmospheric wind and temperature using openly available sources for three ranges of altitude:

- For altitudes above 60 km, the most recent version of the Naval Research Laboratory (NRL) empirical Horizontal Wind Model (HWM; Drob et al., 2015) is applied while the temperature is extracted from the NRLMSISE-00 climatology (Picone et al., 2002).
- For altitudes between 25 and 70 km, we use the NASA Modern-Era Retrospective Analysis (MERRA; Rienecker et al., 2011) both for winds and temperature.
- For the lowest altitudes, up to 35 km, we apply the NCEP / NCAR reanalysis (Kalnay et al., 1996).

In the overlap altitude regions we apply a Hann-weighted average. For temporal and spatial coordinates where the underlying models are not available, we use multi-dimensional linear interpolation between the nearest grid points.

6.3.4 Introducing atmospheric wind perturbations due to gravity waves

It has long since been accepted that ray-tracing procedures through standard atmospheric models are unable to predict many infrasound arrivals which are repeatedly observed in the data. Such so-called shadow zone arrivals are usually interpreted as being caused by fine-scale inhomogeneities, in particular related to the presence of gravity waves (e.g. Gibson et al., 2008). Physics-based models have been sought to model the expected effect of gravity waves on infrasound propagation, and the

spectral model of Gardner et al. (1993) and Gardner (1994) was employed by Gibson et al. (2008) to generate many realizations of an atmosphere perturbed under the influence of gravity waves. Following the approach of Gibson et al. (2008), we generate wave spectra (Gardner et al., 1993; Gardner, 1994) at 4 different altitudes (see Figure 6.3.4).

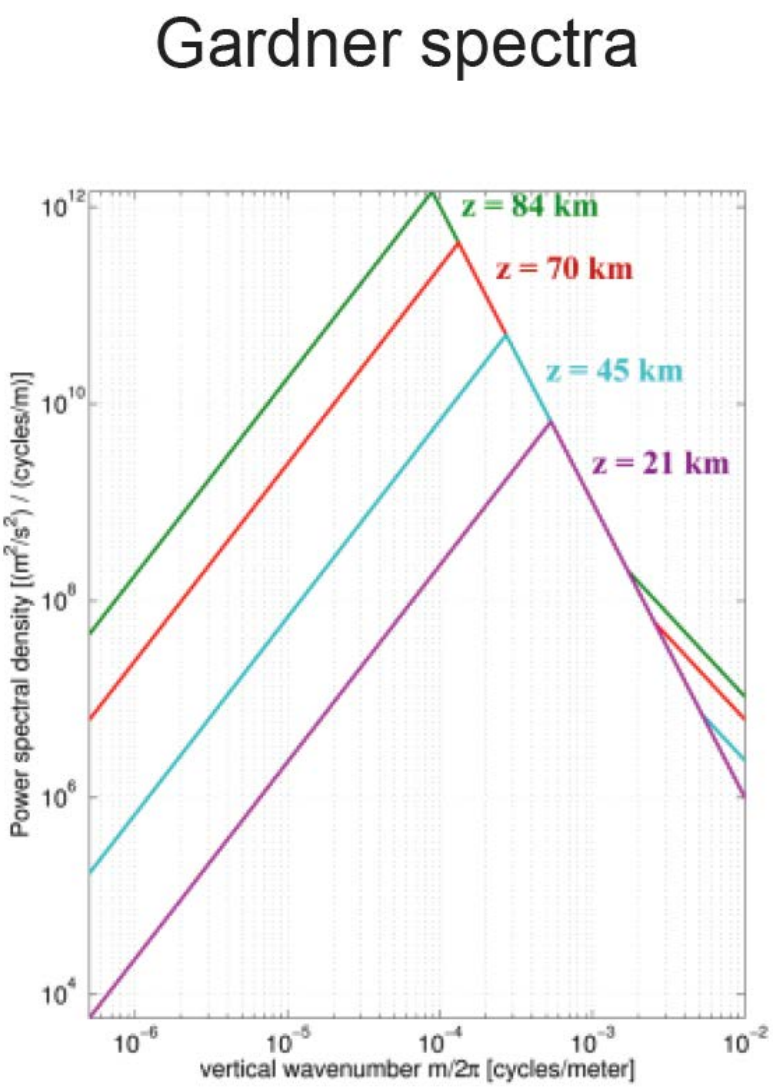

Fig. 6.3.4 Wind perturbation spectra from Gardner's gravity wave model for four different altitudes.

Each spectrum is then multiplied by a random phase factor and inverse Fourier transformed. By using different random phase factors we get different gravity wave realizations. Finally, compound gravity-wave profiles (dependent only upon altitude) are formed by weighted averaging over realizations corresponding to the 4 underlying altitudes. By varying the Gardner spectrum power, we hence vary the amplitude of the wind perturbations (Figure 6.3.5).

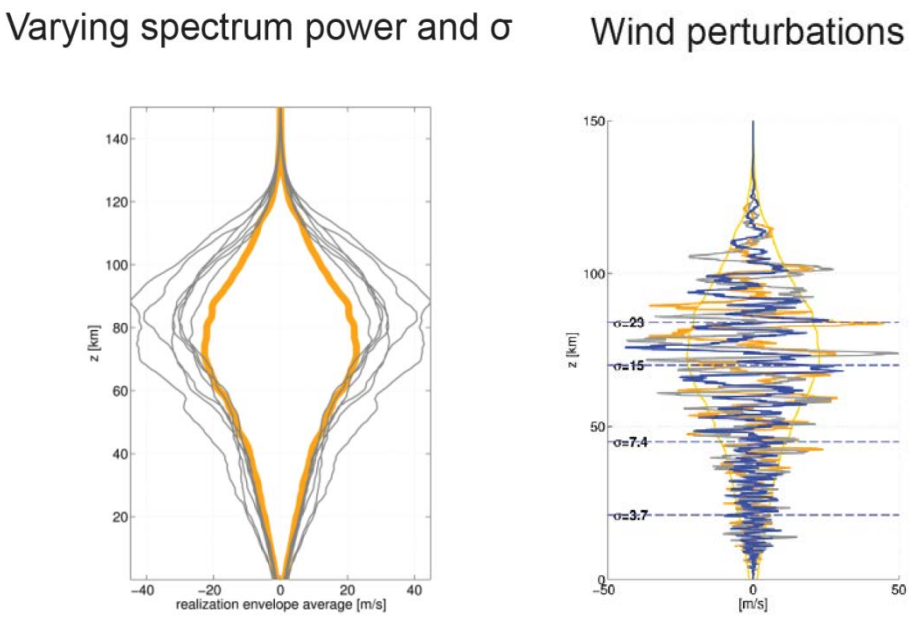

Fig. 6.3.5 Generation of wind perturbations from Gardner spectra. Left: varying spectrum power. Right: different compound realizations of gravity-wave induced disturbances to the wind profile.

6.3.5 Modelling of infrasound propagation in unperturbed models

We see from the data that the occurrence of infrasound arrivals varies from explosion to explosion. The atmospheric model will also change from day to day and we wish to assess the correspondence between the infrasound observed and that predicted to arrive by ray-tracing through a given model. Instead of traveltimes, we consider the celerity: the distance over the ground divided by the time taken. The first-arriving stratospheric signals have a higher celerity than the later arriving thermospheric phases. Figure 6.3.6 displays rays traced through the model with no perturbation for the August 24 explosion. It is clear that only high-altitude (thermospheric) rays reach the array in the unperturbed model.

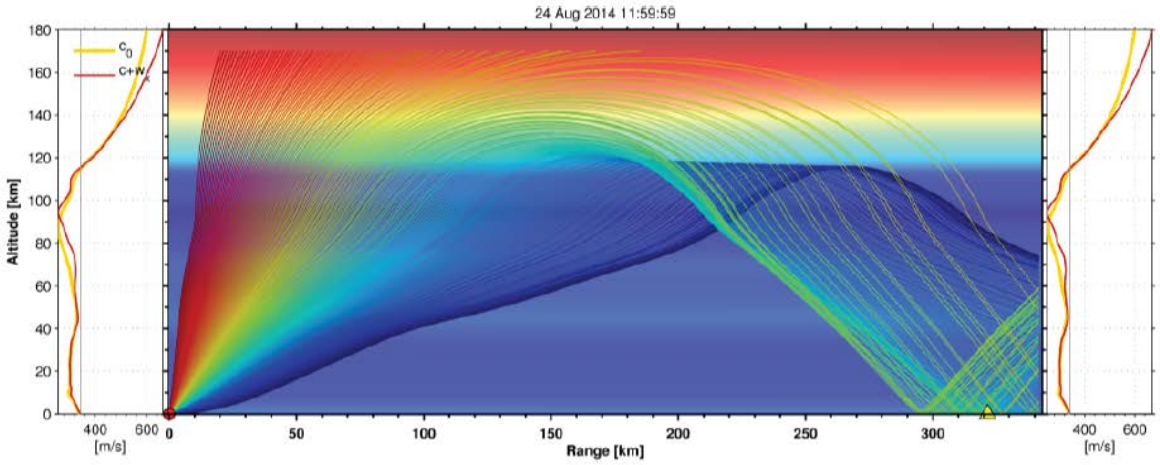

Fig. 6.3.6 Ray-paths obtained using ART2D through the unperturbed atmospheric profile for the August 24 Hukkakero explosion. The yellow triangle at 320 km is the IS37 array.

For each of the 12 largest Hukkakero explosions, we

- calculate celerities of observed coherent high-frequency (HF, 1-6 Hz) and low-frequency (LF, below 1 Hz) energy originating from the explosions.
- calculate celerities of signals modelled using ray-tracing through the atmospheric model at the time of the event.
- calculate the probability that infrasound energy with a given celerity is observed and/or modelled. (This is to say that, for a given celerity, we provide the proportion of the 12 occasions for which an infrasound signal was observed and/or predicted using ray-tracing through the atmospheric model for that time.)

Figure 6.3.7 confirms that, for the unperturbed models at the times of each of the 12 explosions, the only arrivals predicted to reach the array are thermospheric phases. Most of the thermospheric phase predictions are supported by observations although, for a number of events, only low frequency energy is observed. Both low and high frequency energy is observed for celerities between 280 and 300 m/s but none of these observed arrivals are confirmed by ray predictions through the unperturbed atmospheric models.

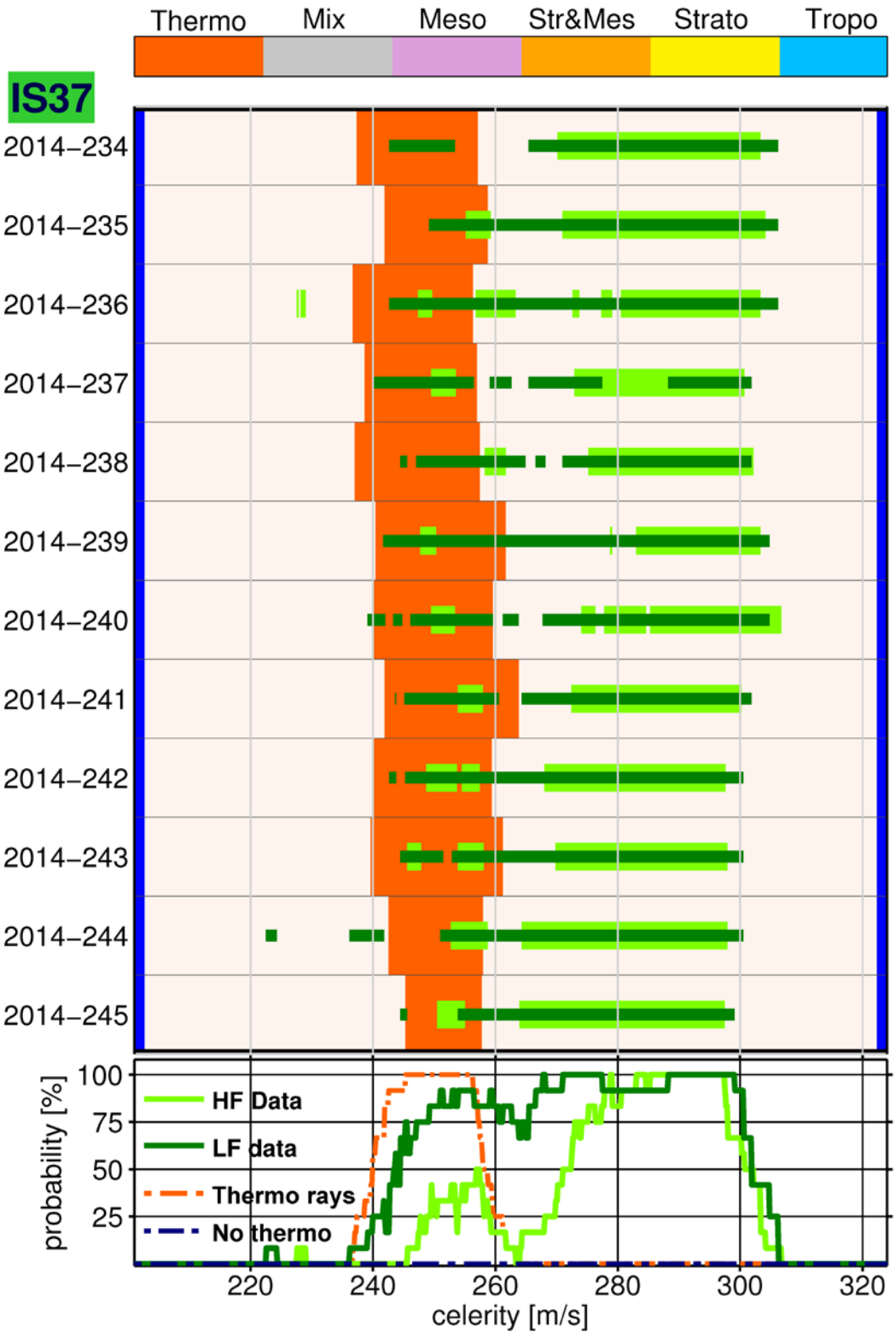

Fig. 6.3.7 Observed infrasound arrivals at IS37 as a function of celerity for the 12 largest Hukkakero blasts in 2014, together with modelled arrivals through an unperturbed atmospheric model. The light and dark green bars indicate respectively high frequency and low frequency infrasound energy actually recorded on the array for each explosion. The remaining colors indicate arrivals at the array that have been predicted by rays along the path indicated by the color. The lowermost panel indicates a probability distribution to indicate how frequently infrasound energy with a given celerity is observed/modelled.

6.3.6 Modelling in perturbed models

We introduced various wind perturbations to the atmospheric models by scaling of the perturbations introduced by Gibson et al. (2008). A large number of realizations were modelled by scaling the Gibson perturbations in the range 0.8 to 2.0.The best fit to the data were found using a scaling factor of 0.8, and the results are illustrated in 3 different realizations shown in the figure below, using the same type of display as above for the unperturbed model.

We see that for all of the events there is a good correspondence between the observed and predicted arrivals.

The lower part of the each panel shows a probability distribution of the observed and modelled celerities. The relatively good correspondence indicates that modelled probability distributions can be used to construct celerity expectation lookup tables which again can be useful in e.g. event location algorithms.

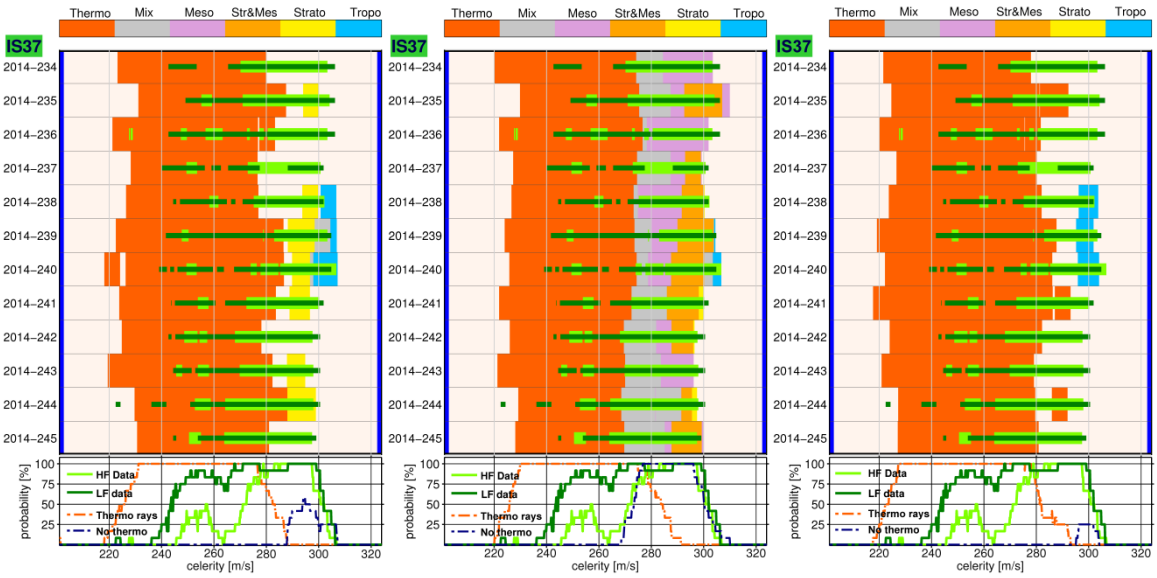

Fig. 6.3.8 Modelling results for 3 realizations of wind perturbations using a scale factor of 0.8 × Gibson.

Figure 6.3.9 further illustrates the great variation in modelled arrivals which can result when adding different perturbation realizations to the atmospheric models with 3 different amplitude scale factors. As expected we see a tendency that increased perturbation amplitude increases the occurrence of modelled returns.

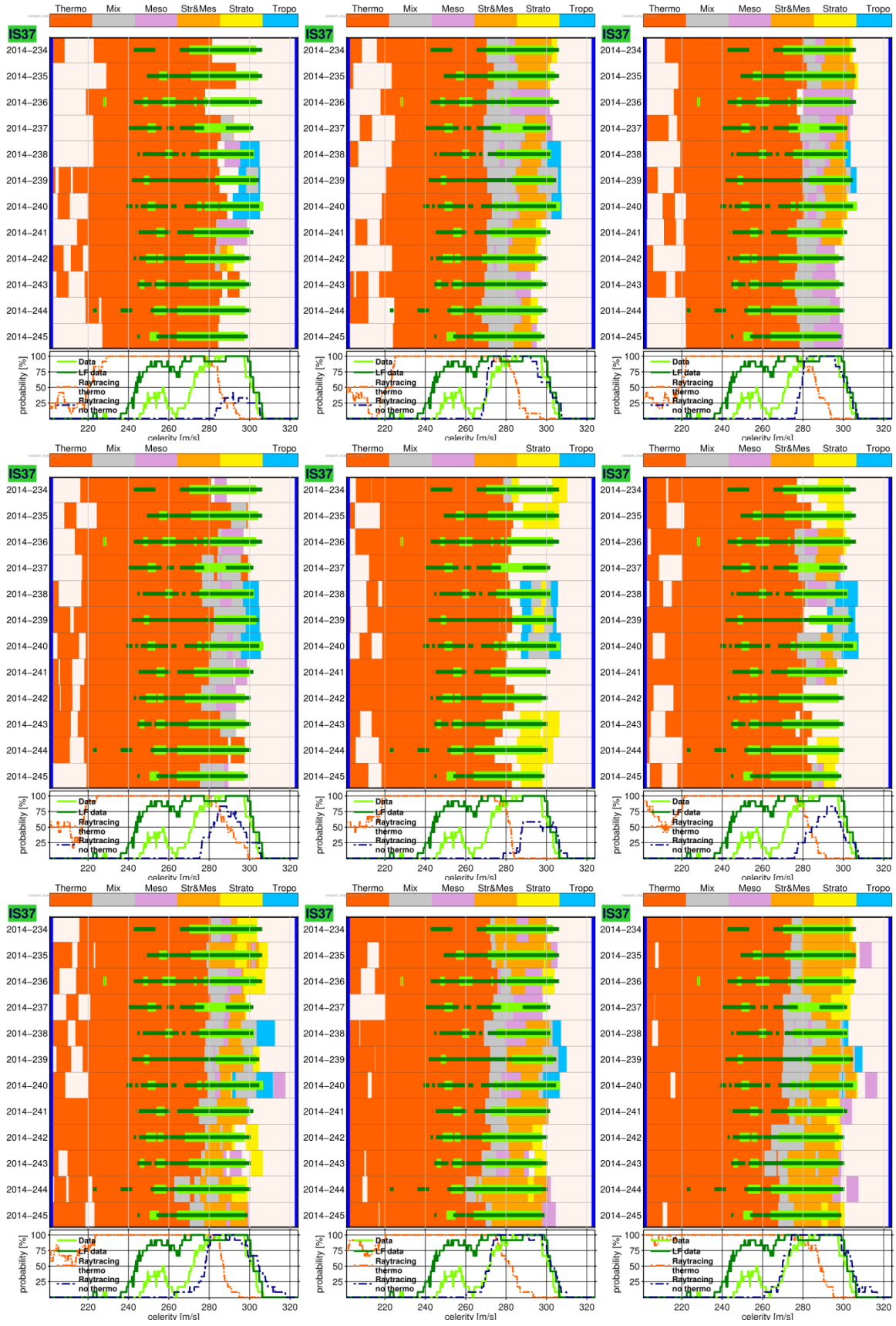

Fig. 6.3.9 Modelling results for 6 realizations of wind perturbations using a scale factor of 1 × Gibson (top row), 1.25 × Gibson (middle row), and 1.6 × Gibson (middle row)

6.3.7 Summary

We consider explosions at Hukkakero in Central Lapland, Northern Finland, from which infrasound was observed at the IS37 infrasound array near Bardufoss in northern Norway. We examine the celerities for which low and high frequency infrasound arrivals are observed and we examine the ability of ray-tracing to predict these arrivals, both in unperturbed atmospheric models and in models where perturbations are added to simulate the effect of gravity waves. Both in the modelling and in the observations, we consider arriving signals not only for the first arrival of each phase, but instead along the full wavetrain. This way we study the full impulse response of the events.

The thermospheric arrivals are predicted using the ray-tracer without the addition of any perturbations to the atmospheric model. However, the perturbations are necessary to be able to predict rays with turning points at stratospheric altitudes. The thermospheric phases are typically of lower frequency and they are not observed at all for the smallest of these events.

Regarding the necessity to include gravity-wave perturbations in the models, we also point out that recent research indicates that small-scale fluctuations are not always necessary to improve the match between predictions and observations (Smets et al. 2015). Smets and co-authors show that applying probabilistic propagation modelling using ensembles of perturbed ECMWF analysis atmospheric models can considerably improve the match.

Moreover, we need to emphasize the ray-tracing method's shortcomings due to its inherent high-frequency assumption, which for example can result in overestimating the width of shadow zones.

By varying the energy of the Gibson spectra and then shooting rays through a large set of corresponding perturbation realizations and finally analyzing the resulting modelled returns with recorded data, we envision the possibility of estimating the strength of the gravity wave activity.

Celerity expectation lookup tables calculated from probability distributions of the gravity-wave perturbed models can be helpful for interpretation of infrasound signals and for improving event location.

S. P. Näsholm
S. J. Gibbons
T. Kværna

References

Brown, D. J., C. N. Katz, R. Le Bras, M. P. Flanagan, J. Wang, and A. K. Gault (2002). Infrasonic Signal Detection and Source Location at the Prototype International Data Centre, *Pure and Applied Geophysics*, 159, 1081-1125, doi:10.1007/s00024-002-8674-2

Drob, D.P.; Picone, J.M.; Garces, M. (2003). Global morphology of infrasound propagation. *J. Geophys. Res*. 108(12), 4680, doi:10.1029/2002jd003307

Drob, D.P.; Garcés, M.; Hedlin, M.A.H.; Brachet, N. (2010). The temporal morphology of infrasound propagation. *Pure Appl. Geophys*. 167, 437–453. doi:10.1007/s00024-010-0080-6

Drob, D. P., Emmert, J. T., Meriwether, J. W., Makela, J. J., Doornbos, E., Conde, M., Hernandez, G., Noto, J., Zawdie, K. A., McDonald, S. E., Huba, J. D. & Klenzing, J. H. (2015). An Update to the Horizontal Wind Model (HWM): The Quiet Time Thermosphere. *Earth and Space Science*. doi:10.1002/2014ea000089

Gainville, O., Blanc-Benon, P., Blanc, E., Roche, R., Millet, C., Le Piver, F., Despres, B., and Piserchia, P. F. (2009), Misty Picture: A Unique Experiment for the Interpretation of the Infrasound Propagation from Large Explosive Sources, in "Infrasound Monitoring for Atmospheric Studies", eds. Le Pichon, A., Blanc, E., and Hauchecorne, A., Springer, pp. 575-598, doi:10.1007/978-1-4020-9508-5_18

Gardner, C. S., Hostetler, C. A. & Franke, S. J. (1993). Gravity wave models for the horizontal wave number spectra of atmospheric velocity and density fluctuations. *Journal of Geophysical Research*, 98 (D1), pp. 1035-1049. doi:10.1029/92jd02051

Gardner, C. S. (1994), Diffusive filtering theory of gravity wave spectra in the atmosphere, *J. Geophys. Res.*, Vol. 99, No. D10. (20 October 1994), pp. 20601-20622, doi:10.1029/94jd00819

Gibbons, S. J.; Ringdal, F.; Kværna, T. (2007). Joint seismic-infrasonic processing of recordings from a repeating source of atmospheric explosions., *J. Acoust. Soc. Am*. 122: EL158-EL164 doi:10.1121/1.2784533

Gibbons, S. J., Asming, V., Eliasson, L., Fedorov, A., Fyen, J., Kero, J., Kozlovskaya, E., Kværna, T., Liszka, L., Näsholm, S. P., Raita, T., Roth, M., Tiira, T. and Vinogradov, Y. (2015). The European Arctic: A Laboratory for Seismoacoustic Studies. *Seismological Research Letters*, Vol. 86, No. 3. (1 May 2015), pp. 917-928, doi:10.1785/0220140230

Gibson, R.G., Norris, D.E., and Drob, D.P. (2008), Investigation of the Effects of Fine-scale Atmospheric Inhomogeneities on Infrasound Propagation. Proceedings of the2008 Monitoring Research Review, Portsmouth, Virginia, September 23-25, 2008, LA-UR-08-05261 Los Alamos National Laboratory, pp. 872-881. http://rdss.info/librarybox/mrr/mrr2008/PAPERS/06-05.PDF

Hedlin, M. A. H. and Walker, K. (2013). A study of infrasonic anisotropy and multipathing in the atmosphere using seismic networks, *Philosophical Transactions of the Royal Society A: Mathematical, Physical and Engineering Sciences* **371**, doi:10.1098/rsta.2011.0542

Israelsson, H. (2013), Recordings from Hukkakero Explosions in 2009 at Infrasound Stations of the IRF Network. Technical Report, *SeismicInfra Research*. https://www.researchgate.net/publication/259267213_Recordings_from_Hukkakero_Explosions_in_2009_at_Infrasound_Stations_of_the_IRF_Network

Kalnay et al. (1996). The NCEP/NCAR 40-year reanalysis project, *Bull. Amer. Meteor. Soc*., 77, 437-470. doi:10.1175/1520-0477(1996)077<0437:tnyrp>2.0.co;2

Liszka, L.; Kvaerna, T (2008) Propagation of infrasound from chemical explosions*, InfraMatics*, March 2008, 1-10

Meriwether, J.; Mesquita, R.; Sanders, S.; Makela, J.; Harding, D.; Fisher, D.; Buriti, R.; Medeiros, A.F.; Drob, D. (2014). Solar cycle and seasonal variations of equatorial thermospheric temperature and winds. 8th Workshop on Long-Term Changes and Trends in the Atmosphere

Mutschlecner, J. P. and R. W. Whitaker (1999). Thermospheric Infrasound Signals, in "Proceedings of the 21st Seismic Research Symposium, Las Vegas, NV, September 21-24, 1999: Technologies for Monitoring The Comprehensive Nuclear-Test-Ban Treaty", Volume II, LA-UR-99-4700 Los Alamos National Laboratory, pp. 151-158. http://rdss.info/librarybox/mrr/srr1999/papers5/mutschle.pdf

Picone, J.M.; Hedin, A.E.; Drob, D.P.; Aikin, A.C. (2002). NRLMSISE-00 empirical model of the atmosphere: Statistical comparisons and scientific issues. *J. Geophys. Res*., 107(A12), 146, doi:10.1029/2002ja009430

Rienecker, M. M. et al. (2011), MERRA: NASA's Modern-Era Retrospective Analysis for Research and Applications. *J. Climate*, 24, 3624–3648. doi:10.1175/jcli-d-11-00015.1

Smets, P.S.M., L.G. Evers, S.P. Näsholm and S.G. Gibbons (2015), Probabilistic infrasound propagation using realistic atmospheric perturbations, *Geophys. Res. Lett. (1 July 2015),* 2015GL064992. doi: 10.1002/2015gl064992

Walker K. (2012) Atmospheric ray tracer 2D (ART2D). The software was obtained from the site http://sail.ucsd.edu/~walker/software/ART2D/art2d.html although this page has since been discontinued.

Whitaker, R. W. and J. P. Mutschlecner (2008). A comparison of infrasound signals refracted from stratospheric and thermospheric altitudes, *Journal of Geophysical Research* **113**, D08117, doi:10.1029/2007jd008852